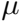
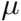
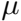


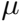
Contents

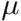
List of Figures

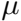


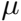


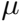


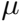




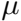








List of Tables



Chapter 1

Literature Review

Review Iterative

1.2 Introduction

1.2.1 Spine

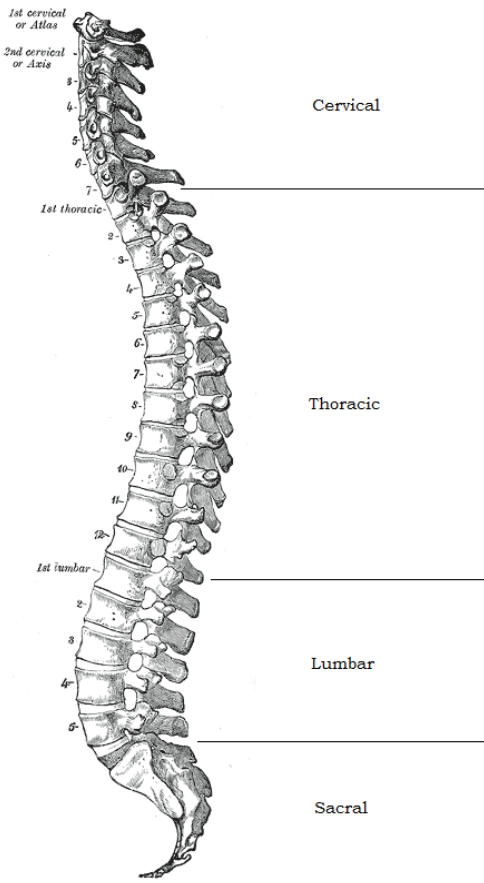


Figure 1.2.1: Curvature of the vertebral column with the four regions labelled. Adapted from [1].

1.2.2 Vertebræ

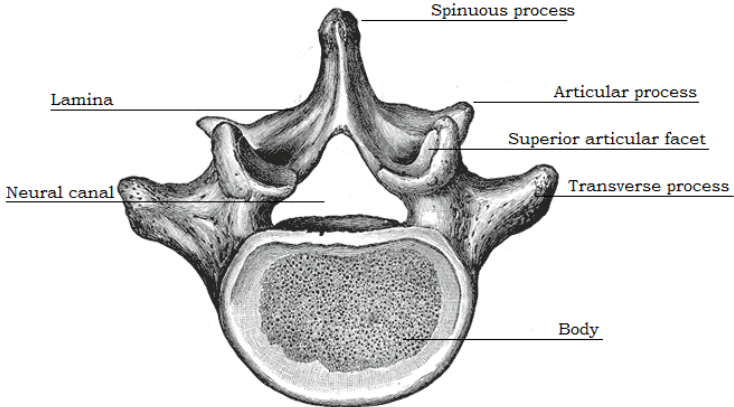


Figure 1.2.2: Superior view of a lumbar vertebrae, identifying the key features. Adapted from [1].

Vertebral Fractures & Vertebral Proplasty 1.3

1.3.1 Vertebral Fracture Types



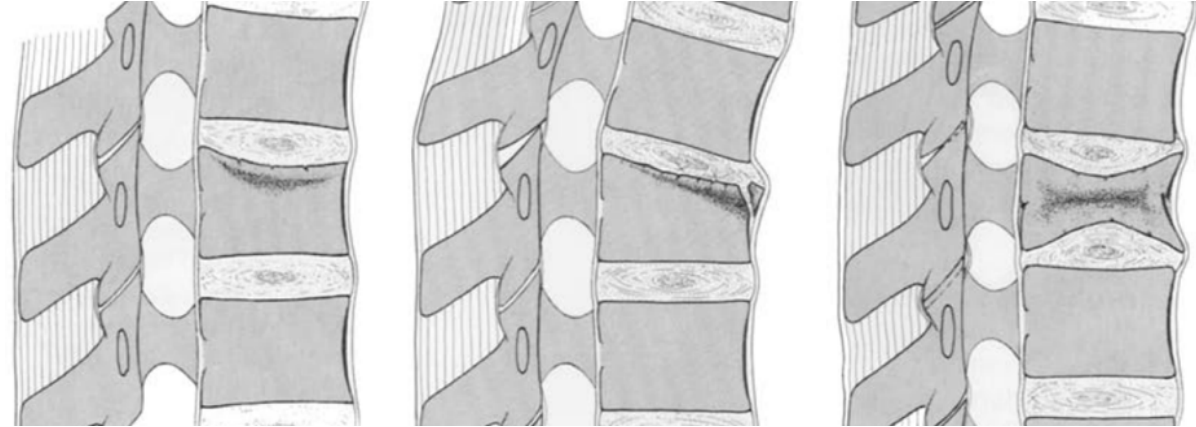


Figure 1.3.1: Types of VCF. Left: Superior end-plate impact. Middle: superior wedge fracture. Right: Vertebral body collapse. Adapted from [2].



1.3.2 Risk Factors

1.3.3 Diagnosis

1.3.4 Vertebroplasty

As fast as vectorized code

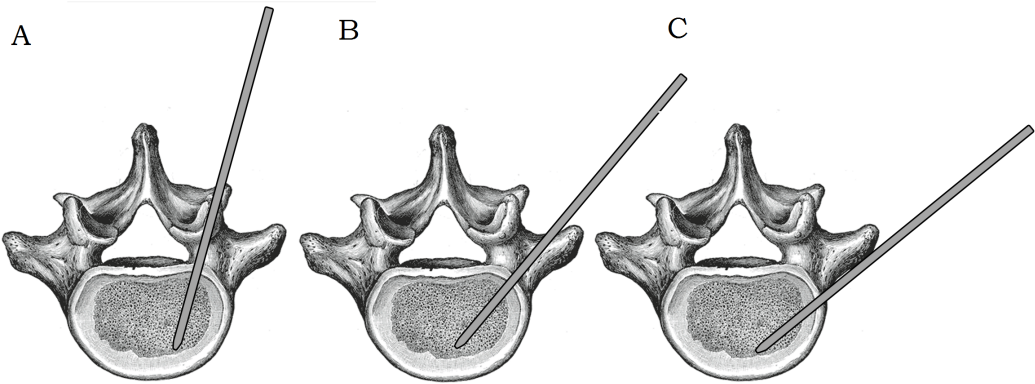
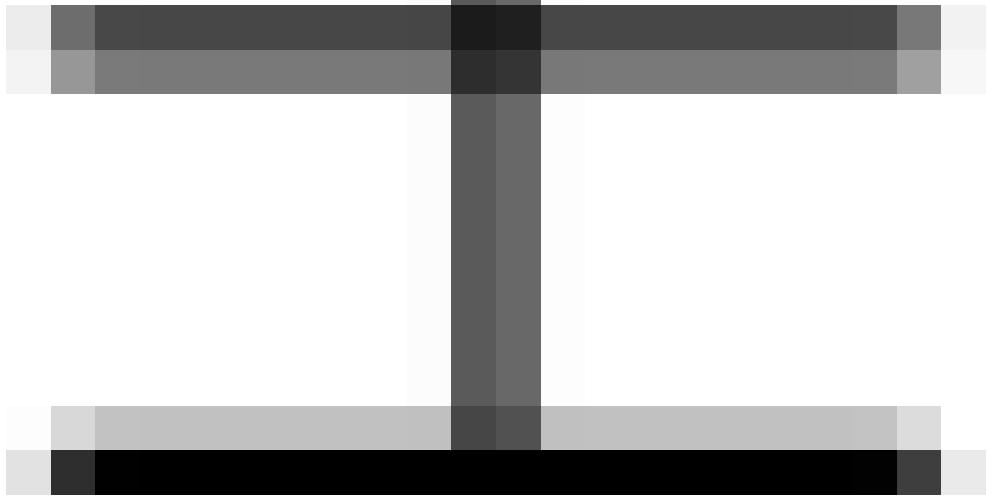


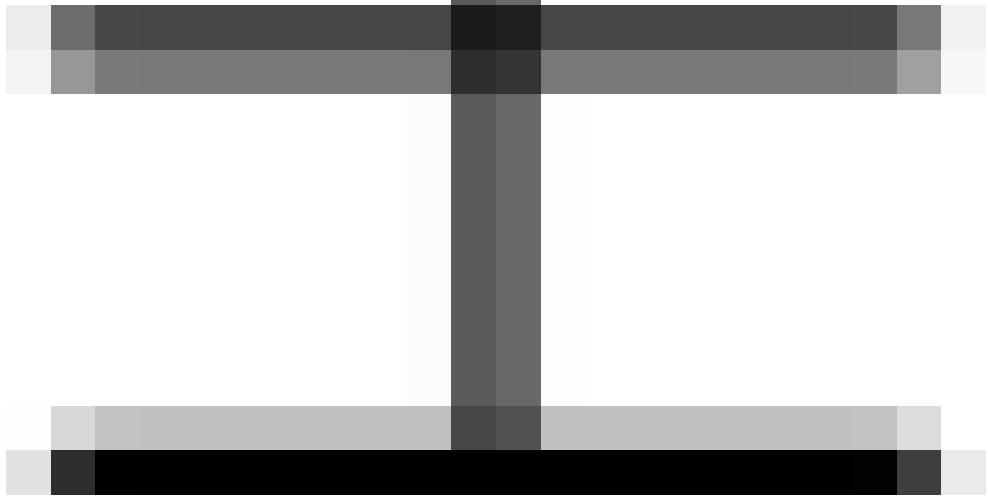
Figure 1.3.2: Three approaches to vertebroplasty. A, transpedicular approach, B, parapedicular approach, C, oblique approach. Adapted from [1].

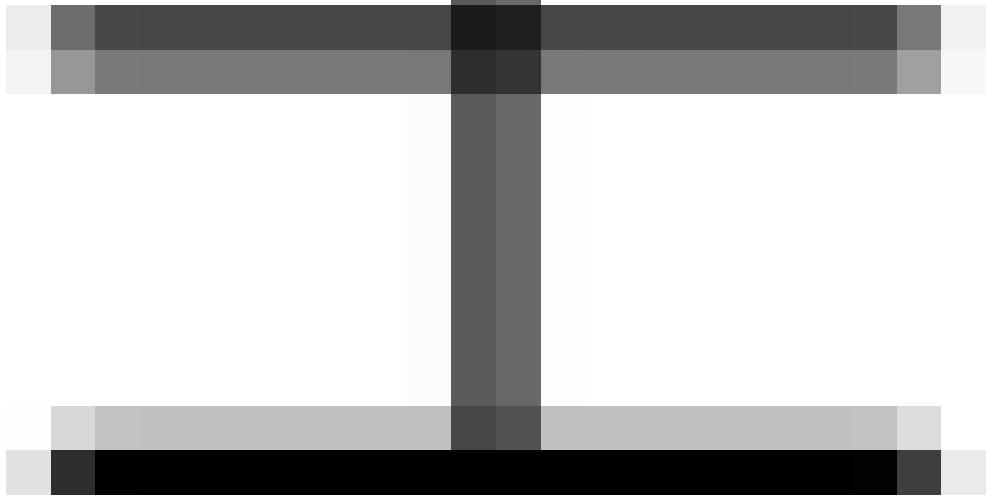
Table 1.3.1: Two randomised clinical trials, with their similar inclusion and exclusion criteria and results for the study.

Study Author	Number of patients	Type of pathologies	Inclusion Criteria	Exclusion Criteria	Results for osteoporotic patients
Buchbinder et al. [23]	71 patients, 35 in VP group, 36 in placebo group	Vertebral compression fractures	Pain < 12 months duration and presence of one or two vertebral fractures	> 90 % collapse, presence of spinal cancer, retropulsion of fragments, hip fracture or infection	No beneficial effect of vertebroplasty over a sham procedure at 1 week or at 1, 3, or 6 months among patients
Kallmes et al. [24]	131 patients, 68 VP group and 63 placebo group	Vertebral compression fractures	> 50 years of age 1–3 painful, osteoporotic vertebral compression fractures between vertebral levels T4 and L5. Fracture < 1 year old	Evidence of neoplasm, retropulsion of fragments, hip fracture or infection	No significant difference between groups one month after the procedure on measures of back pain intensity, functional disability, and quality of life

Wetlands and Global Climate Change

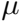


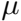


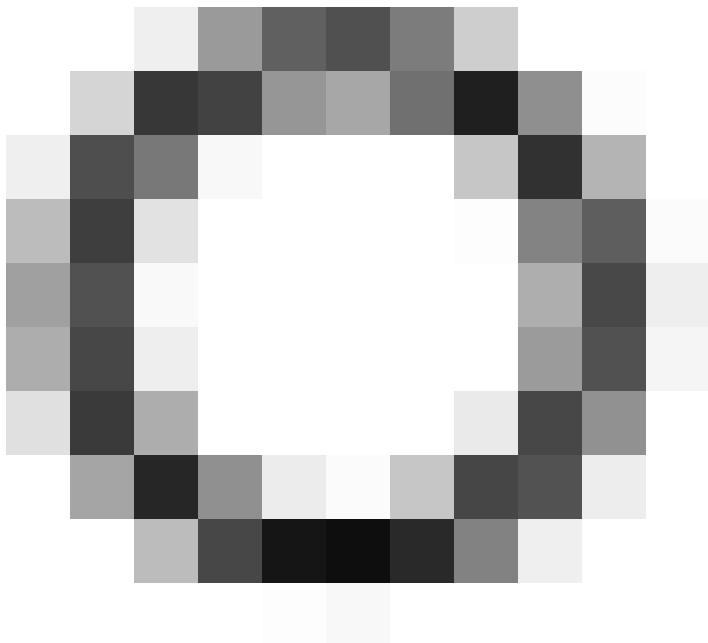


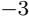
1.4 Experimental Studies

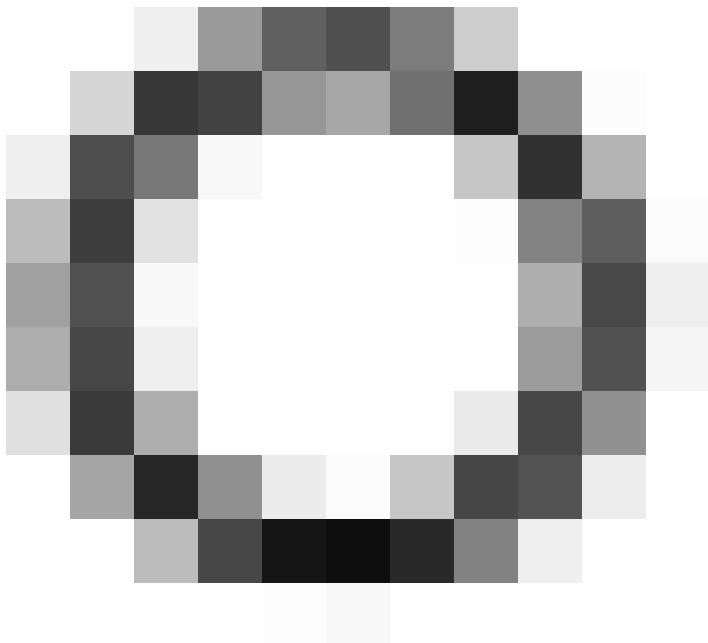
1.4.1. Tabular Structure

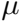


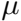


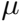












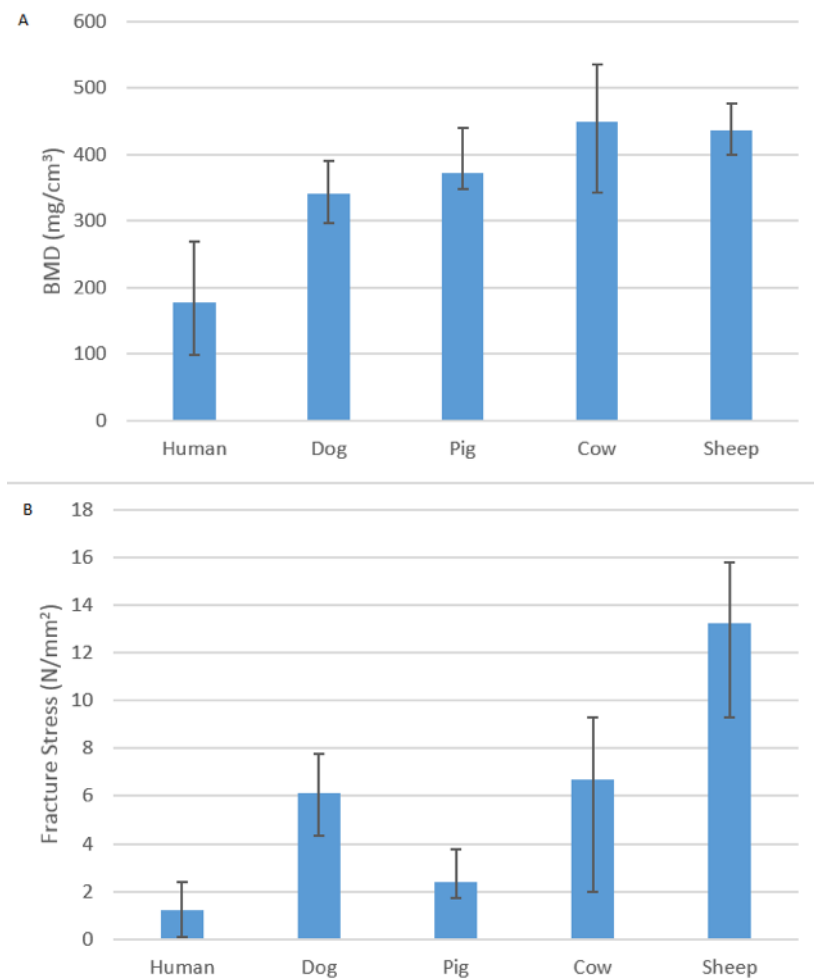
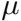
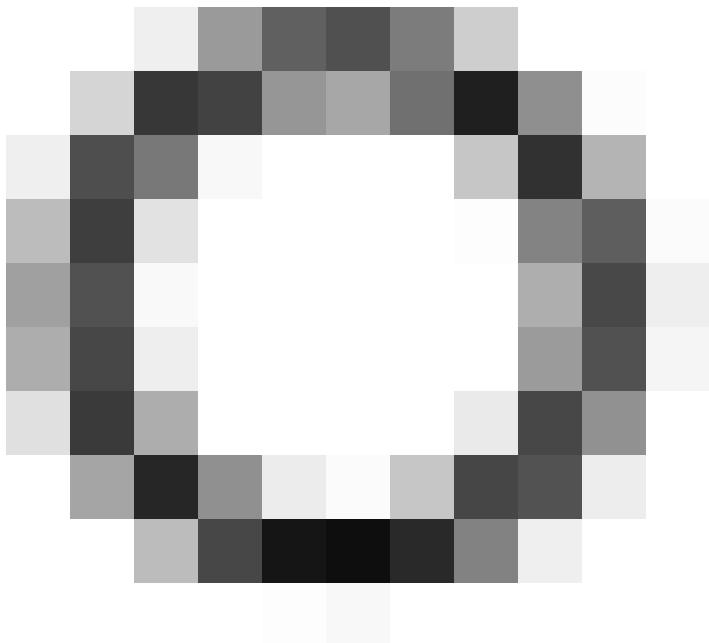


Figure 1.4.1: A, the mean BMD from cylindrical cores taken from the lumbar spine of five different species. B, the mean fracture stress for the same five samples. Bars indicate the range of values. Adapted from [3].

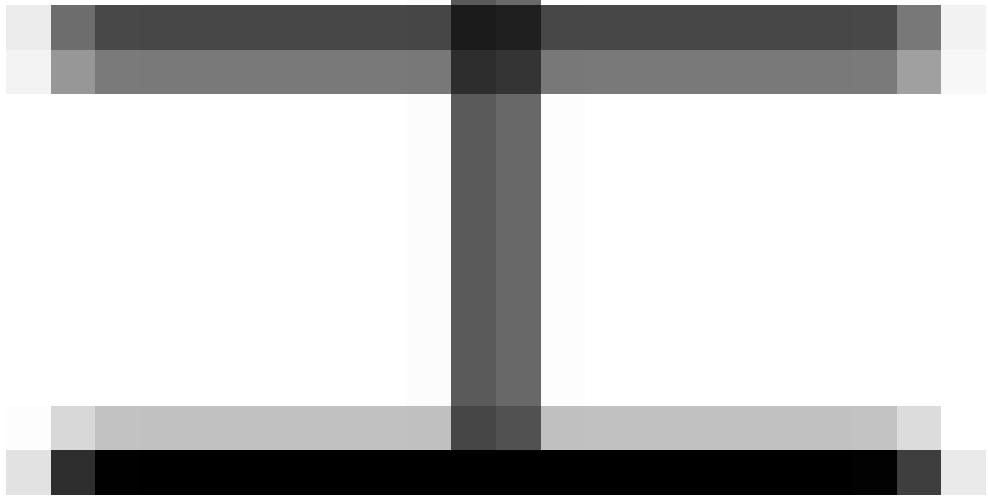
Lección 10







Clouds of Adhesive Mechanical

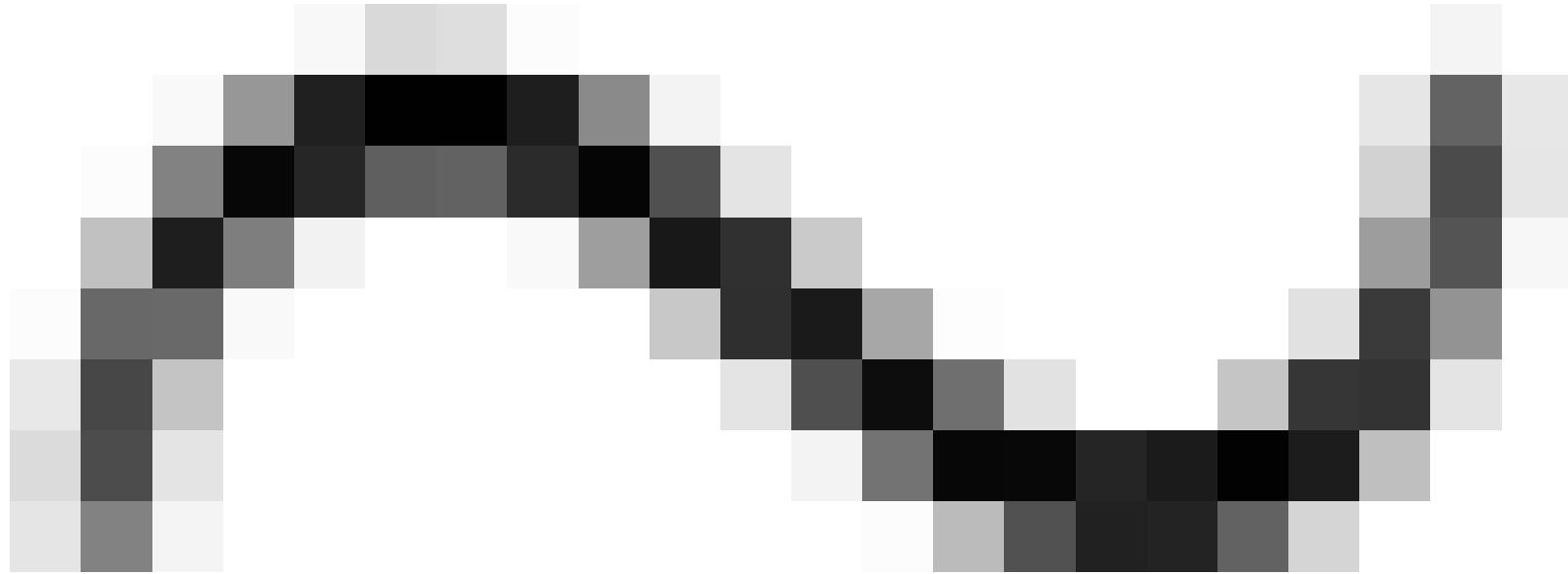


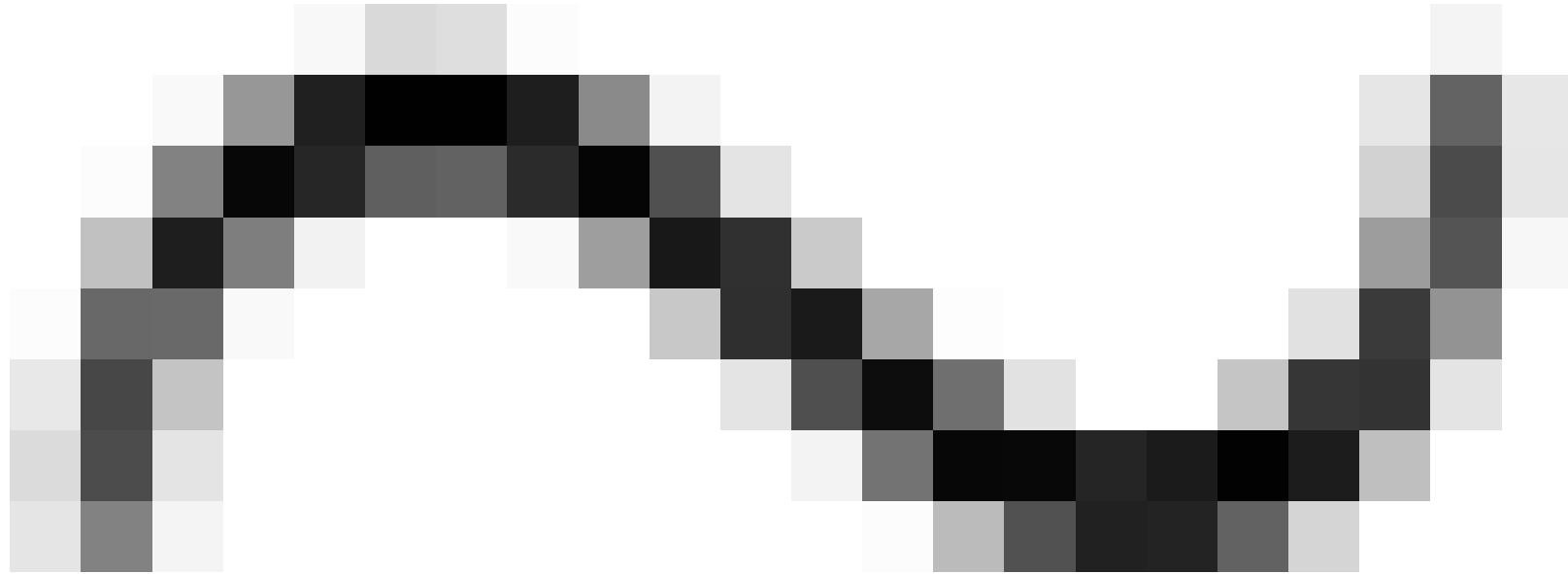
Vertebrates associated with coastal wetlands

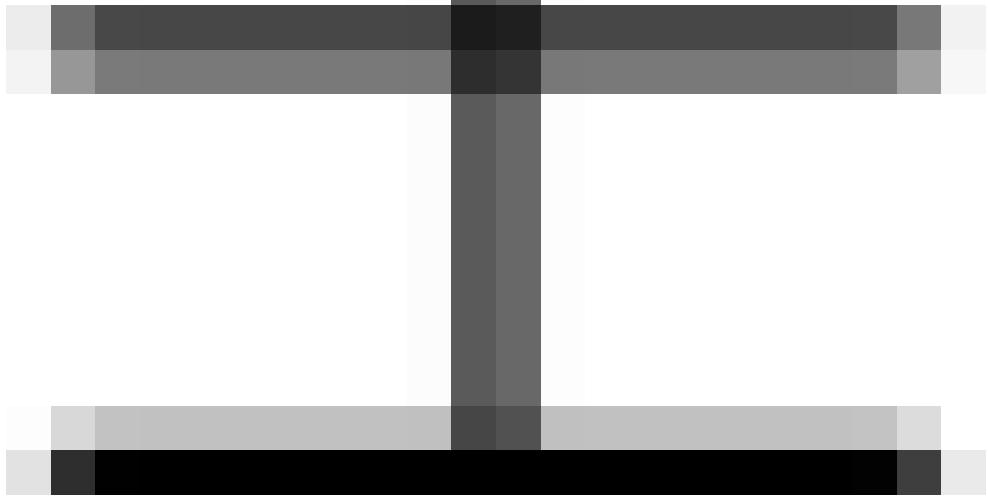
Topoast 1000 feet West 1000 feet East 1000 feet South 1000 feet North

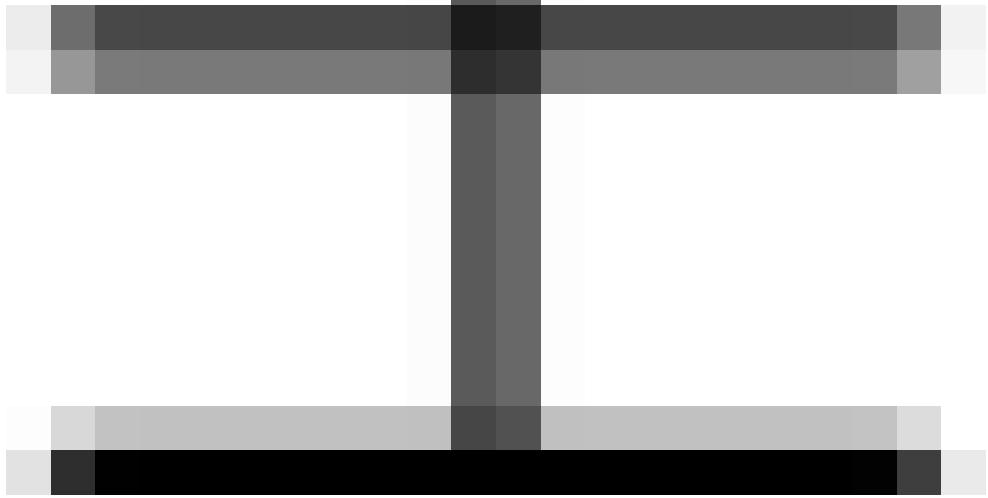
Table 1.4.1: Comparison of the methods used in studies carrying out vertebroplasty experimentally on cadaveric specimens.

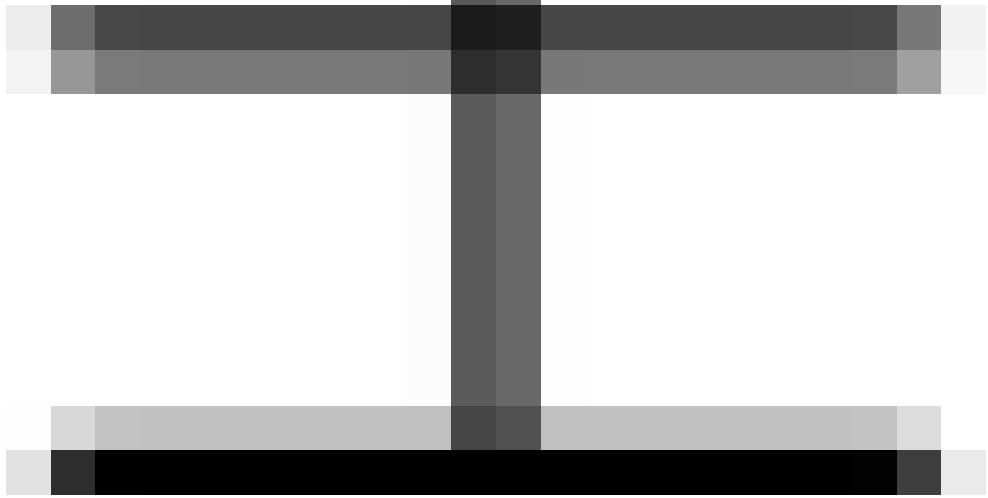
Author	Type of specimen	Procedure type & fill volume	Cement Type	Key Finding
Belkoff et al. [51]	Five vertebral bodies (L1–L5) from four female cadaveric spines (age, 80 ± 5 years)	Transpedicular, 6 ml fill volume throughout	A bioactive cement, Orthocomp (Orthovita, Malvern, PA) & a PMMA based cement, Simplex P (Howmedica, Rutherford, NJ)	Significantly greater strength following injection of cement, compared to the intact vertebrae
Furtado et al. [43]	Twenty-six single vertebrae from 2 female cadavers (age, 88 and 89 years)	Extrapedicular into anterior third of vertebral body, 20 % volume fill, based on height x endplate surface area	PMMA with 20 % by dry weight of barium sulfate	Increased failure strength by a factor of 1.72 post vertebroplasty compared to the intact vertebrae
Higgins et al. [52]	Human cadaveric, 61 vertebrae from 5 cadavers with mean age of 81 years	Unipedicular, 10% and 20% cement fill by volume, with unfilled as controls	PMMA	A statistically significant 36% strength increase as compared with the unfilled controls regardless of density levels
Pneumaticos et al. [48]	40 vertebrae from four human cadaveric thoracic spines (age range 65-69 years)	Transpedicular, 6 ml fill volume throughout	PMMA, with 5 to 1 ration of barium sulphate	A reduced failure load post vertebroplasty, although non-significant



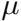


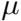




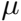


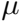
1.5 Finite Element Modeling (FEM)

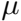


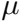


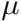
1.5.1 Geometry & Meshing

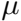


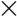


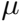


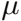


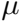


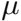


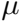


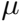


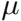


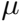


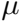


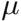


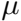












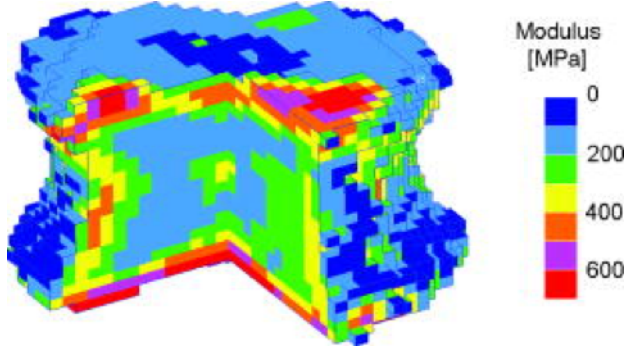
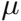
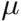
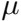


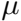
Figure 1.5.1: Voxel finite element mesh of L2 vertebrae used by Buckley et al. with voxel size of 2 mm [4].

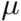


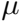


1.5.2 Material Properties









1.5.3 Modeling Vertebroplasty

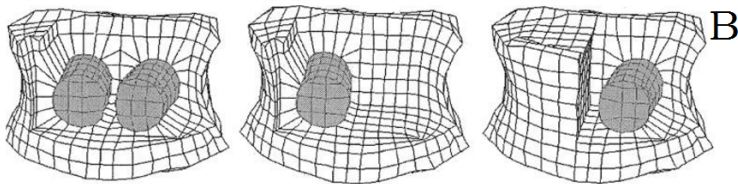
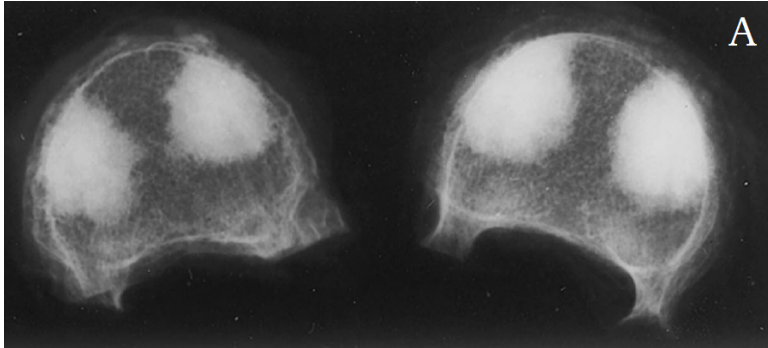
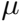


Figure 1.5.2: A: Top view μ CT scans of human vertebrae augmented *in vitro*, showing gradual reduction of cement opacity to the edges of the internal cement volume, adapted from Belkoff et al. [5]. B: The augmented model generation for the study carried out by Liebschner et al. [6].



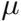
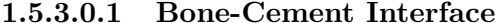
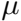
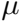


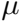
Table 1.5.2: Method of geometry generation, cement position, location and materials used for five finite element studies of vertebroplasty.

Author	Geometry	Cement position & shape	Cement material
Baroud et al. [67]	Hand modelled , described in Smit et al. 1997, two level model	Used 70% fill of cement	Used previously obtained values for cement infiltrated bone, 46 times stronger, 12 times stiffer than surrounding trabecular bone.
Chevalier et al. [69]	μ CT scanned pre and post augmentation, model of vertebroplasty combined cement region with non-augmented scan.	Cement position and structure taken directly from μ CT scans	Bone-cement mixture described by a rule of mixture using a tensor for the isotropic stiffness and for bone stiffness.
Liebschner et al. [6]	Taken from μ CT data	Cement capsule design, cylinder with rounded edges. Positioned to investigate uni/bipedicular vertebroplasty and centred cement positioning.	Unspecified, PMMA
Polikeit et al. [68]	Taken from CT scans at 1 mm resolution, manually constructed details not visible. Two level model	Cement modelled as barrels using radiographs as guides. Positioned to investigate uni/bipedicular vertebroplasty including one model with 100 % fill	Constant Young's modulus (3000 MPa) & Poisson ratio (0.41)
Wijayathunga et al. [41]	μ CT scanned post augmented vertebrae	Identified from μ CT scan using constant threshold value based on greyscale	Used constant properties for Young's modulus and yield stress. Examined effect of lowering cement modulus to align with that of cement impregnated bone

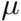


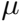






Dissertation studies 1.5.4





1.6 Capture of Variation in Population

6.1 Principal Component Analysis Methods

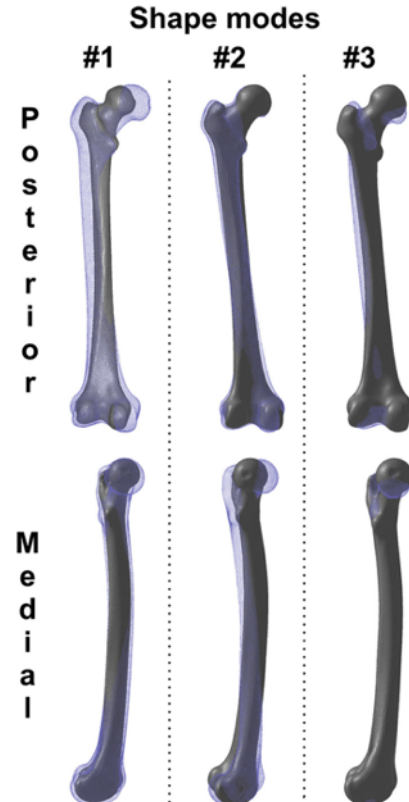
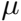


Figure 1.6.1: Femoral shape variations for the first three modes from the PCA. From 115 bones the maximum eigenvalue is shown with the minimum eigenvalue shown in wireframe. Taken from [7].

1.6.2 Discussion

1.7 Conclusion



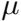
1.8 Aims & Objectives

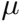
Chapter 2

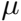
Bovine Tail Vertebrae

2.1 Experimental Methods

2.1.1 Introduction







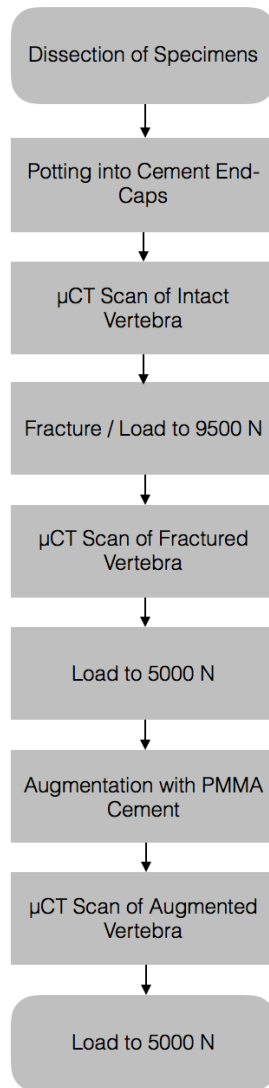
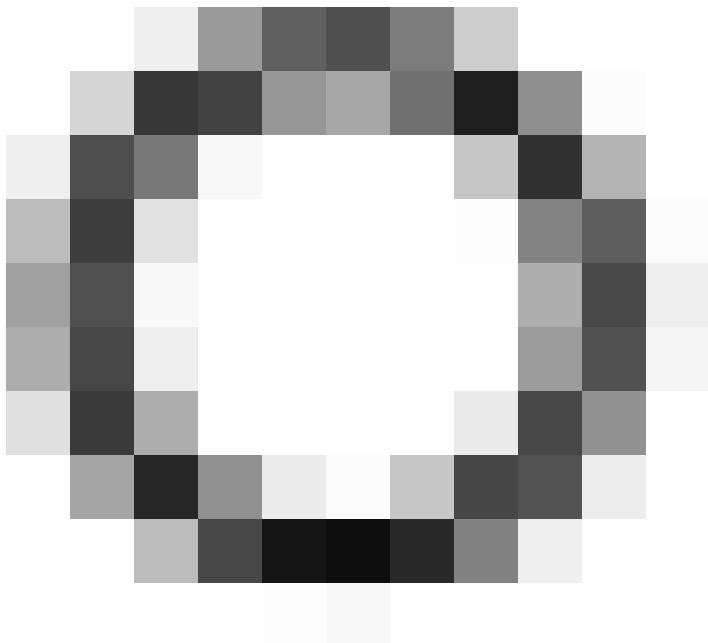
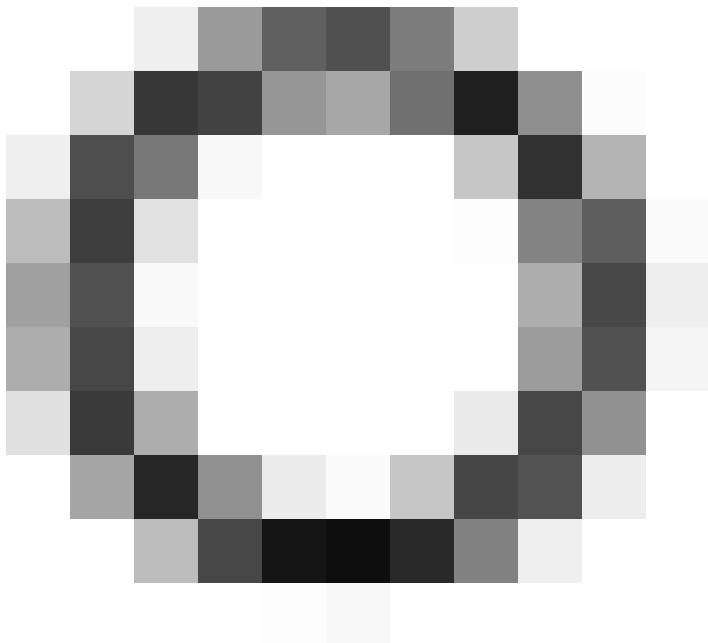
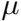


Figure 2.1.1: Flow-chart detailing the experimental process from initial dissection to final load test.

2.1.2 Specimen Preparation







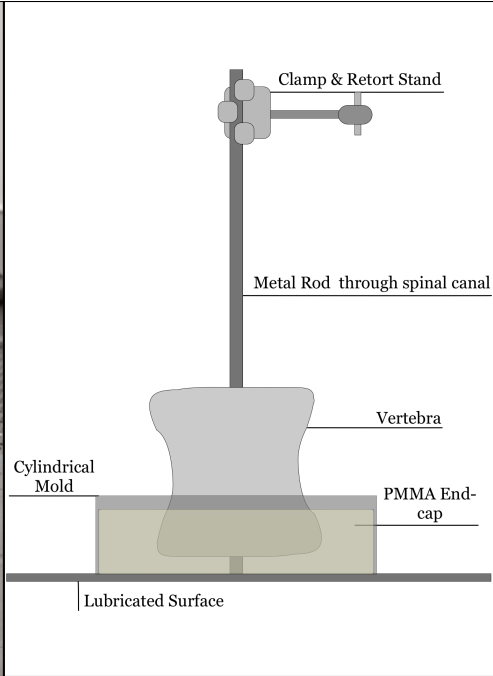
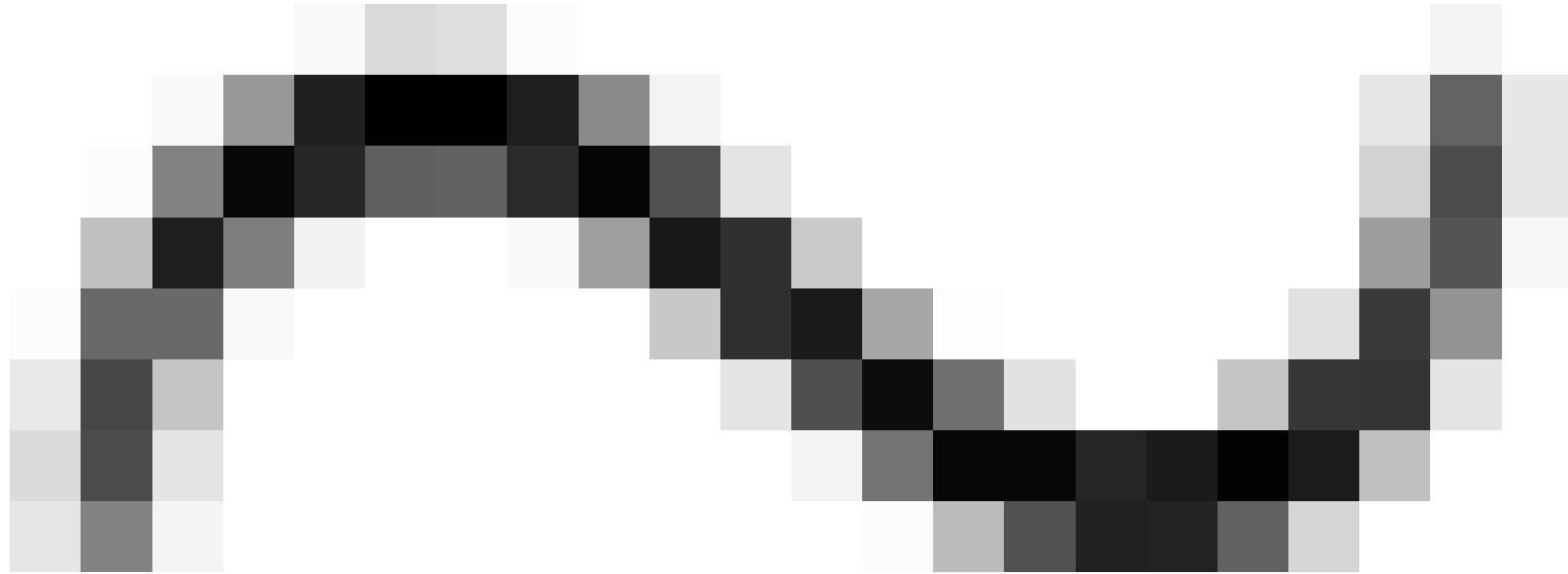


Figure 2.1.2: Photograph and diagram depicting the method of creating end-caps for the specimens.



2.1.3 Axial Compression

2.1.3.1 Fraction Creation

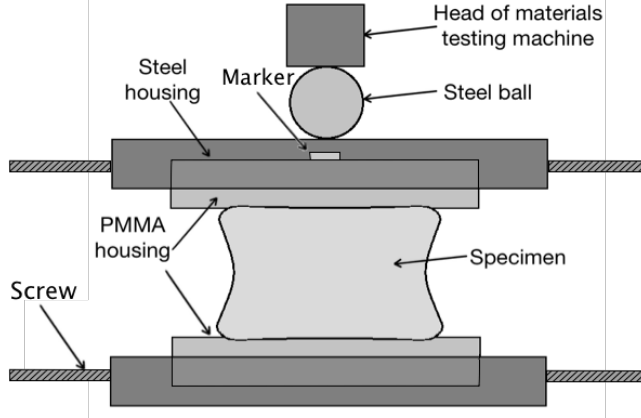


Figure 2.1.3: The experimental setup for axial loading the vertebral specimens.

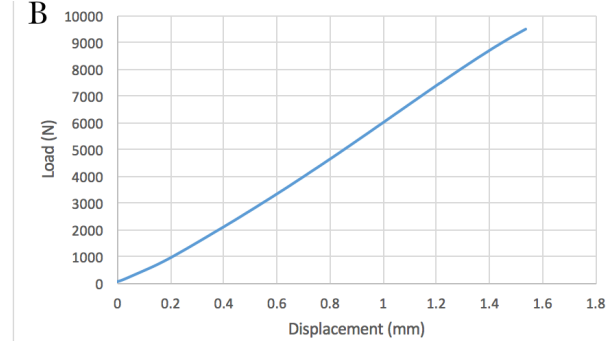
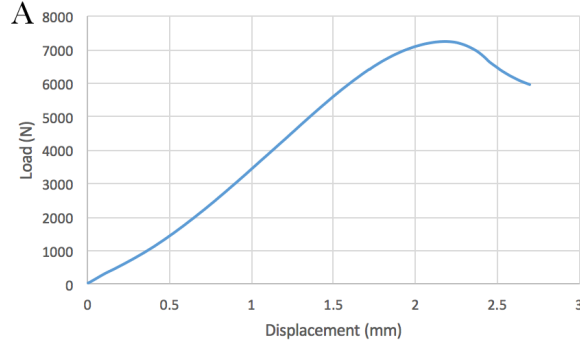


Figure 2.1.4: The difference between failure (A) and non-failure (B) for bovine tail vertebra compressed to a maximum load of 9500 N or until a peak was observed.

Post-tensioned Roadways & Pavement Construction

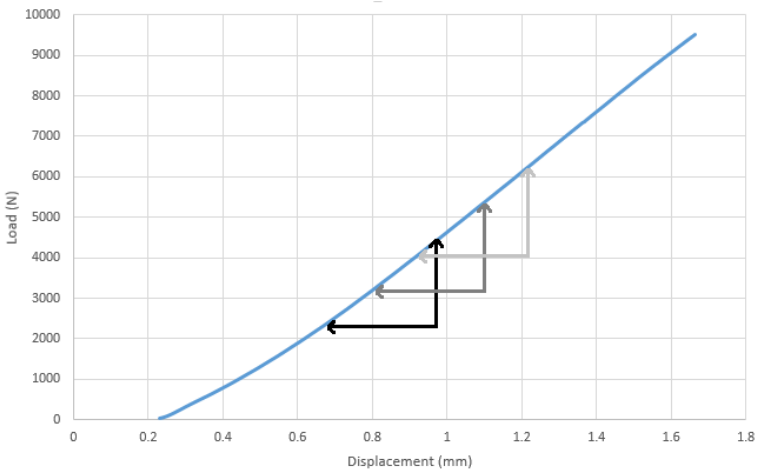


Figure 2.1.5: A typical load displacement curve showing how the gradient was taken from 0.3 mm long sections incremented at 0.1 mm across the length of the curve.

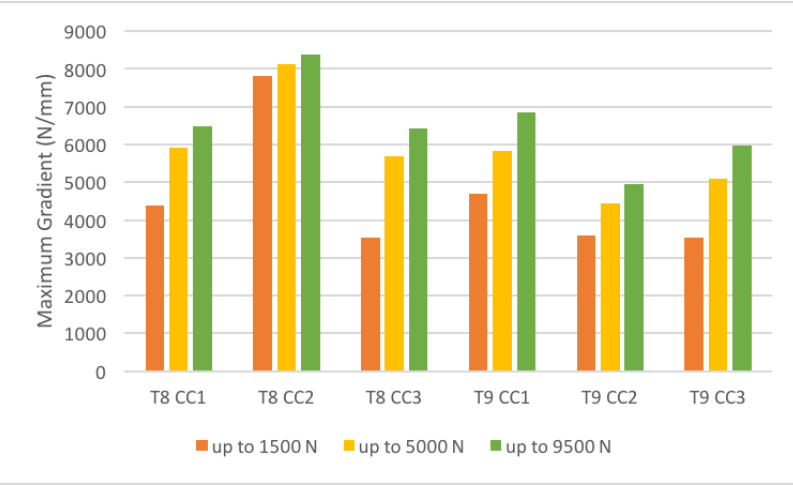
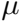
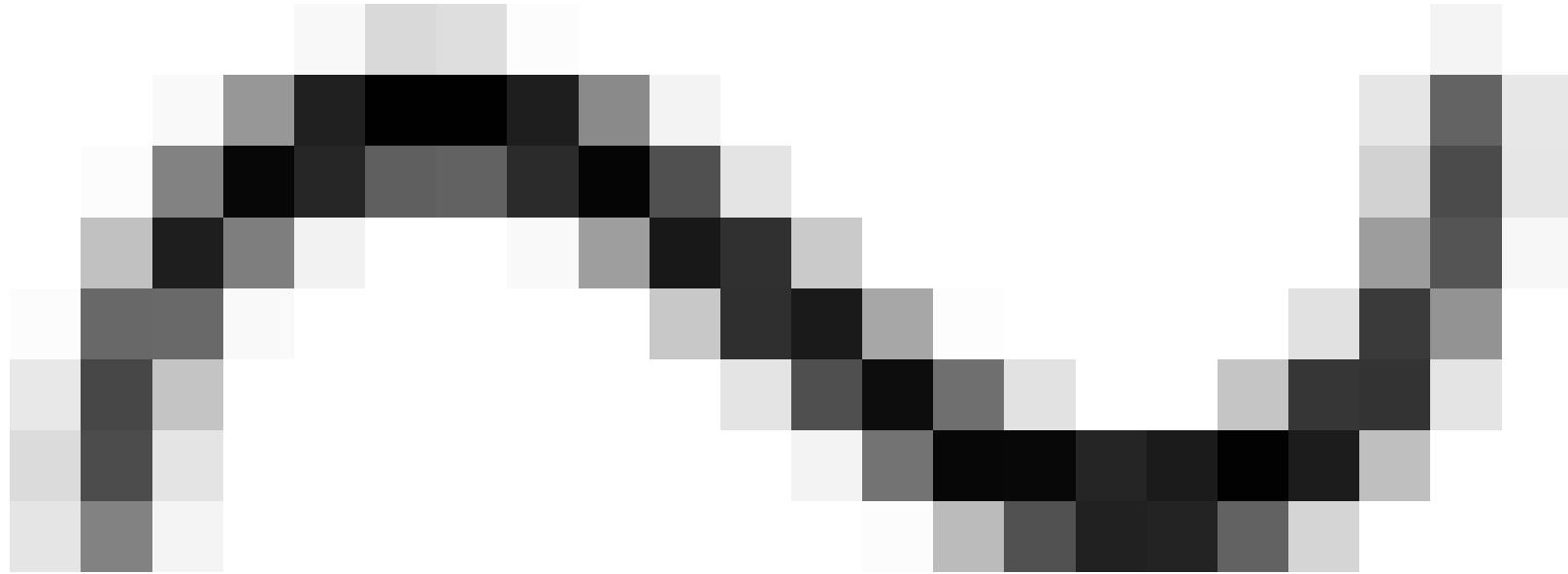


Figure 2.1.6: The difference seen when measuring the greatest gradient (stiffness) using different portions of the load displacement curve. From 0 to 1500 N, 0 to 5000N and 0 to 9500N.

2.1.4 Vertebroplasty

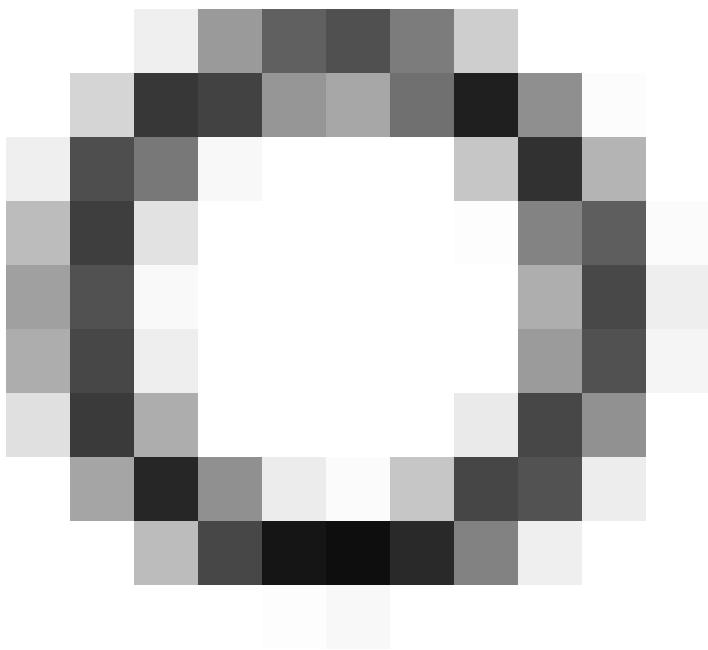


2.1.4.1 Initial Procedure

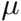


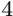
2.1.2 Changes and Additions to the Procedures and Applications

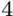


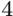


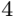
Two additional

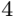












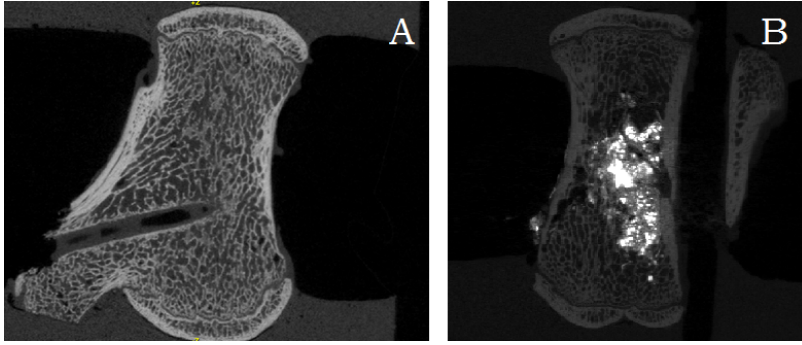


Figure 2.1.7: A: μ CT scan of an augmented vertebrae, with some visible PMMA residing in the needle channel. B: μ CT scan of an augmented vertebrae using PMMA mixed with barium sulphate.

Introducción

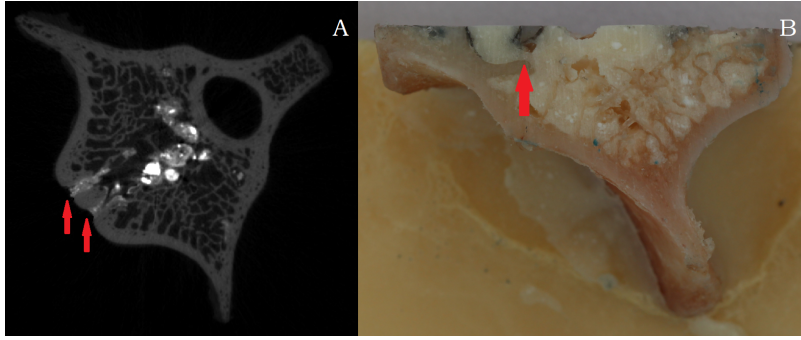


Figure 2.1.8: A: μ CT scan of an augmented vertebrae showing the cement leaking from vascular channels on the anterior side. B: Photograph of an augmented vertebrae cut into four quarters showing a vascular channel leading into the spinal canal.

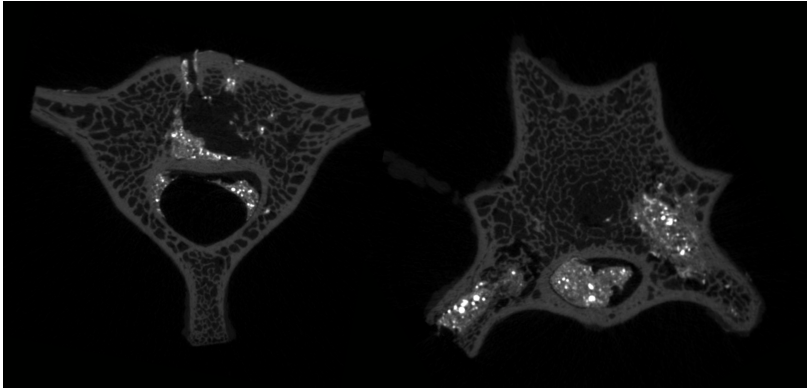
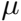
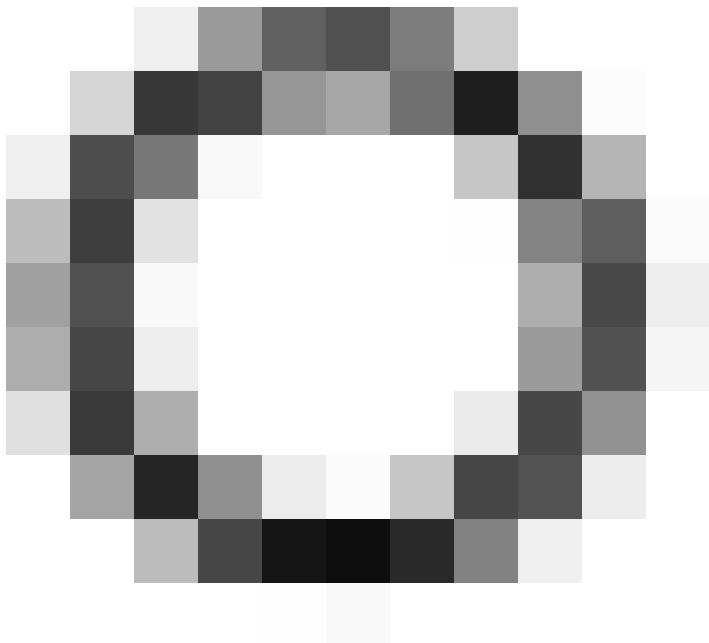
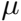


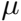
Figure 2.1.9: μ CT scans of two vertebra, showing the cement leaking into the spinal canal and out of the vascular channels and the vertebral surface.

2.1.5 MicroCT Scanning









2.1.6 Results

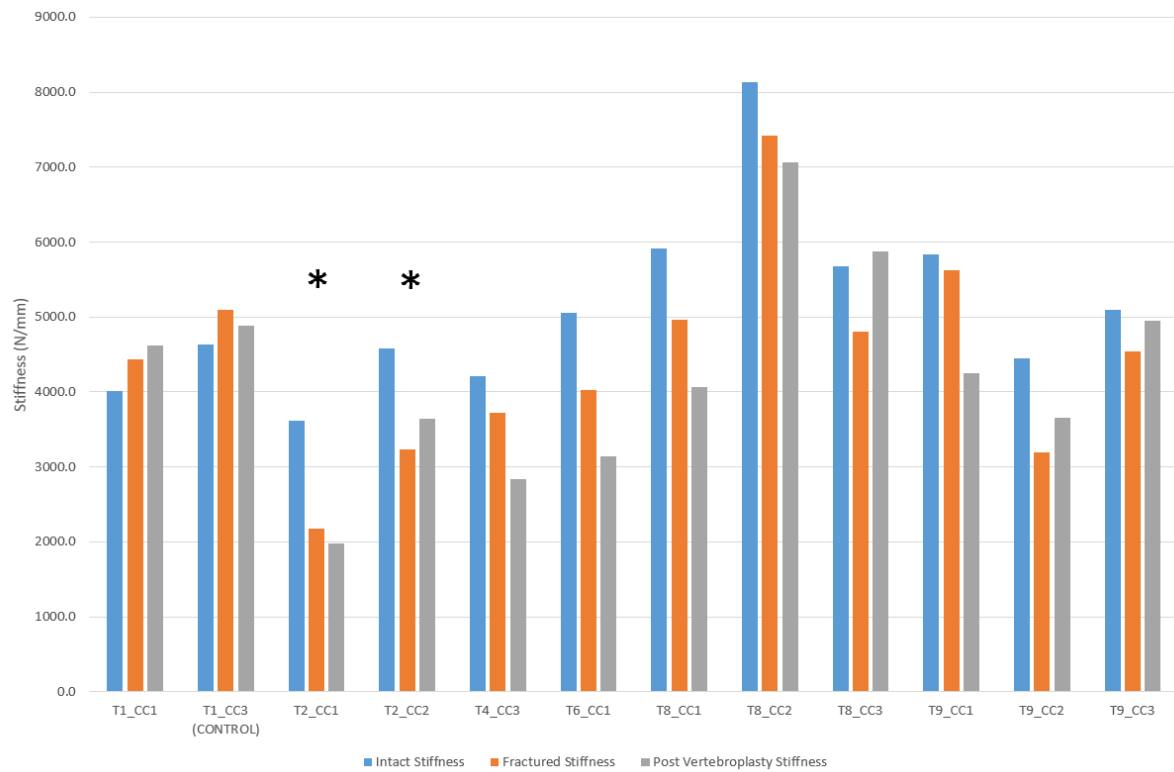


Figure 2.1.10: The maximum stiffness of 12 bovine tail vertebrae between 0 and 5000 N taken from load - displacement data. Showing the stiffness of the intact vertebrae, a post - fracture stiffness and a post - vertebroplasty stiffness for each. * Indicates those specimens that achieved a clear failure below 9500 N.

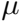


Table 2.1.1: The volume of cement and the vertebra volume for the 12 specimens used, along with the percentage cement fill and an indication as to whether the stiffnesses of the augmented vertebrae were greater than the fractured stiffness. This information was measured from the down-sampled models generated from μ CT scans of the vertebrae.

Vertebrae	Cement Volume (mm ³)	Vertebra Volume (mm ³)	Cement Percentage of Vertebra Volume (%)	Increase in Augmented Stiffness over Fractured Stiffness
T1 CC1	2260	32440	6.97	*
T1 CC3	465	27039	1.72	
T2 CC1	663	23285	2.85	
T2 CC2	3405	20373	16.71	*
T4 CC3	1363	25446	5.36	
T6 CC1	830	29332	2.83	
T8 CC1	1257	37357	3.36	
T8 CC2	4489	29248	15.35	
T8 CC3	1041	28403	3.67	*
T9 CC1	2922	45681	6.40	
T9 CC2	2210	38894	5.68	*
T9 CC3	2437	35840	6.80	*

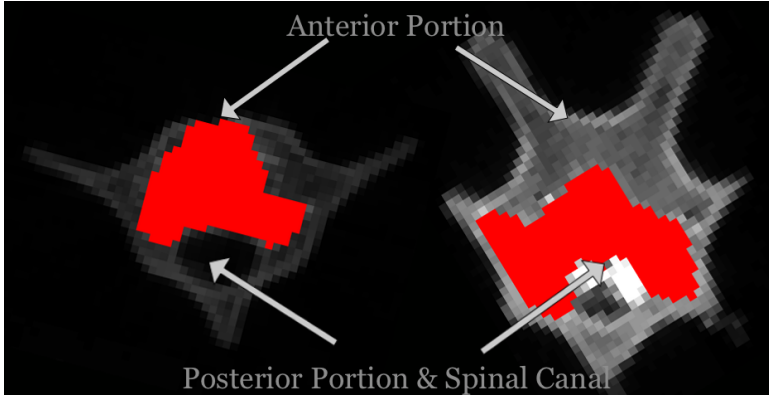


Figure 2.1.11: μ CT scans of T2-CC2 (left) and T8-CC2 (right), with cement masked in red, showing the extend of cement fill at the point where the cement was most anterior.

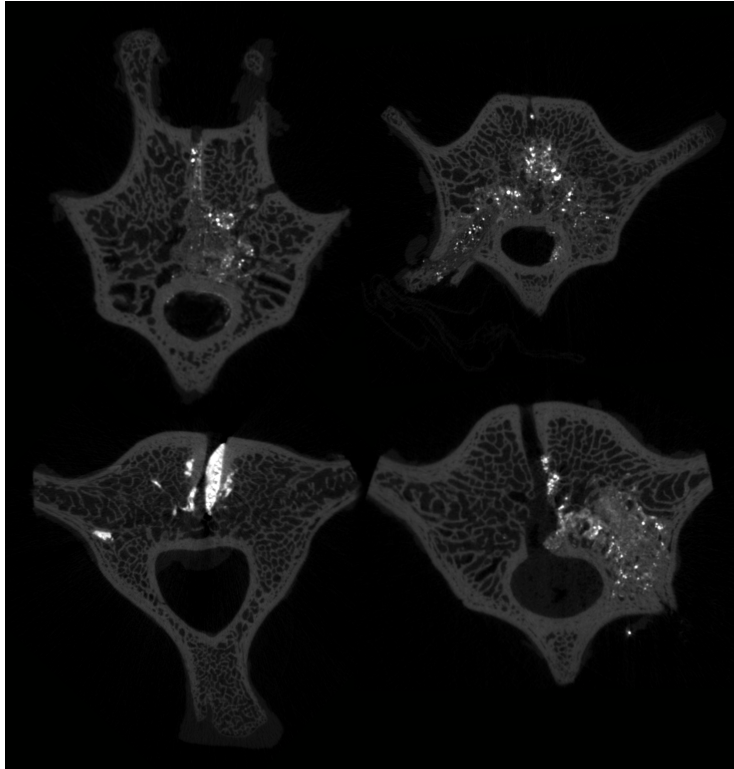


Figure 2.1.12: μ CT scans of four augmented vertebra using a steel rod to fill the spinal canal and blu-tac to cover the external vascular channels. Shows greatly reduced cement content within the spinal canal with less cement at the surface of vascular channels.

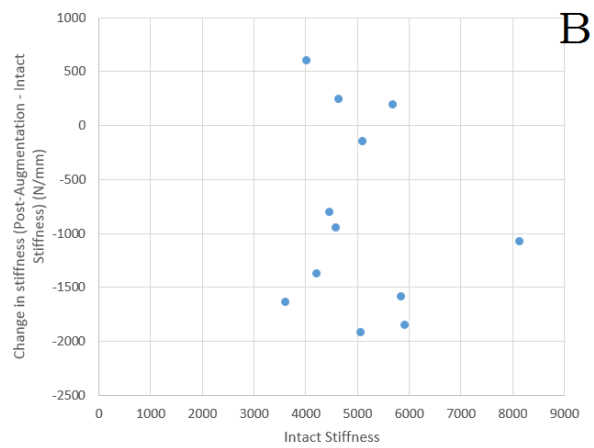
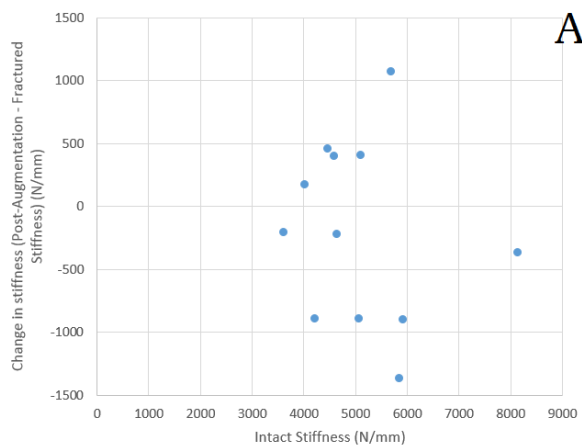
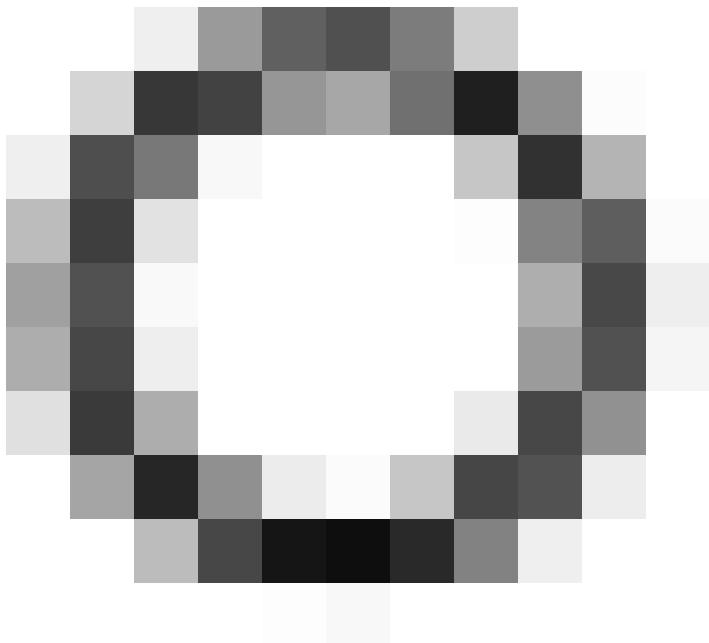
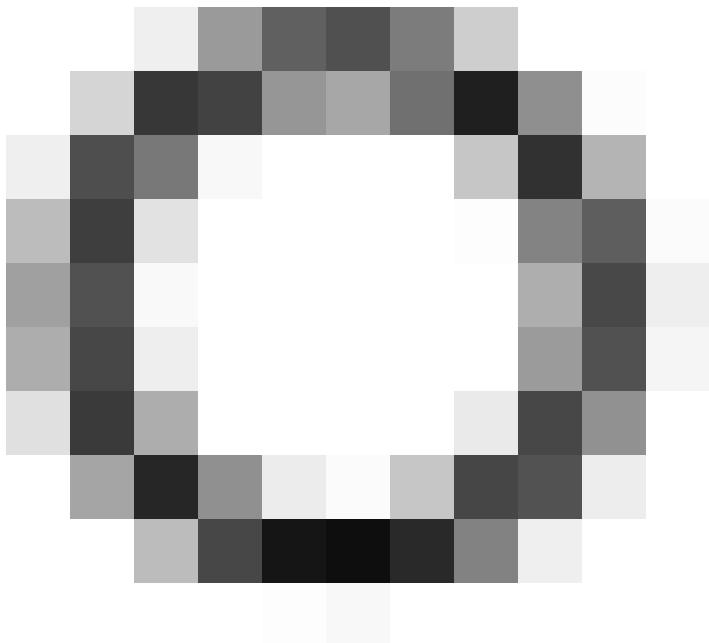


Figure 2.1.13: A: The difference between the post augmentation and fractured stiffness against the intact stiffness. B: The difference between the post augmentation and intact stiffness against the intact stiffness.

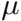
2.1.7 Discussion

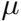


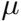


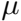
2.2 Finite Element Modelling Methods

2.2.1 Model Creation









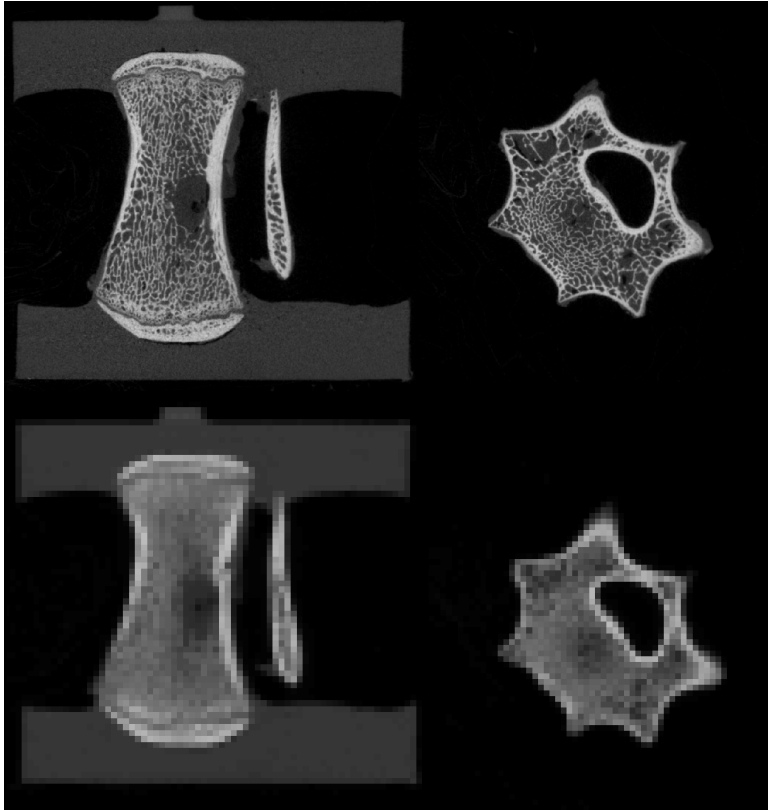


Figure 2.2.1: Side and top view of a vertebral μ CT scan showing the effect of the downsample from $82 \mu\text{m}$ to 1mm cubed.

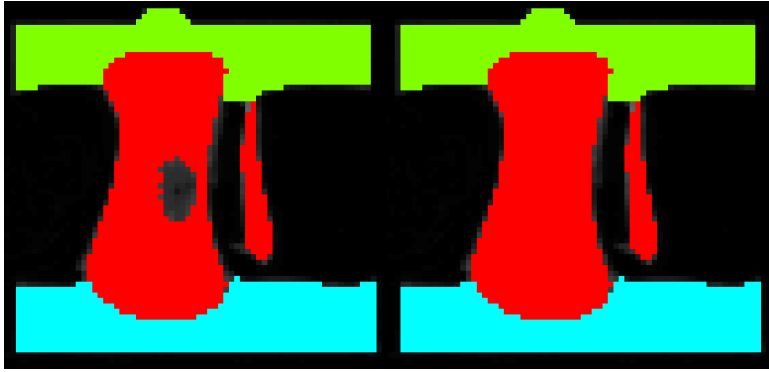
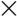
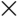


Figure 2.2.2: Side view of a vertebral model showing segemented vertebra, including the internal void that is filled.





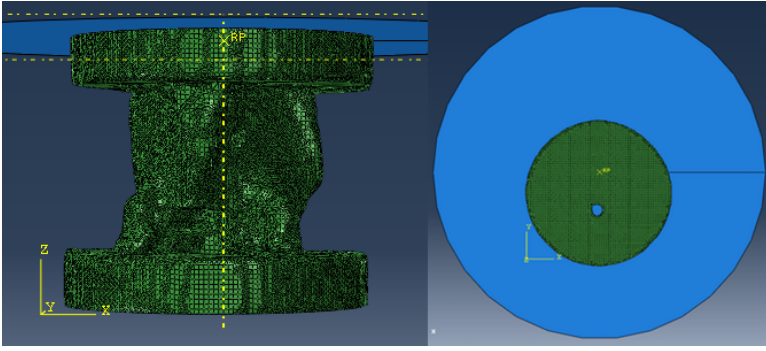


Figure 2.2.3: Side & top down view of a vertebral model showing the alignment of the analytical rigid plane.

2.2.1 Augmented Model Generation

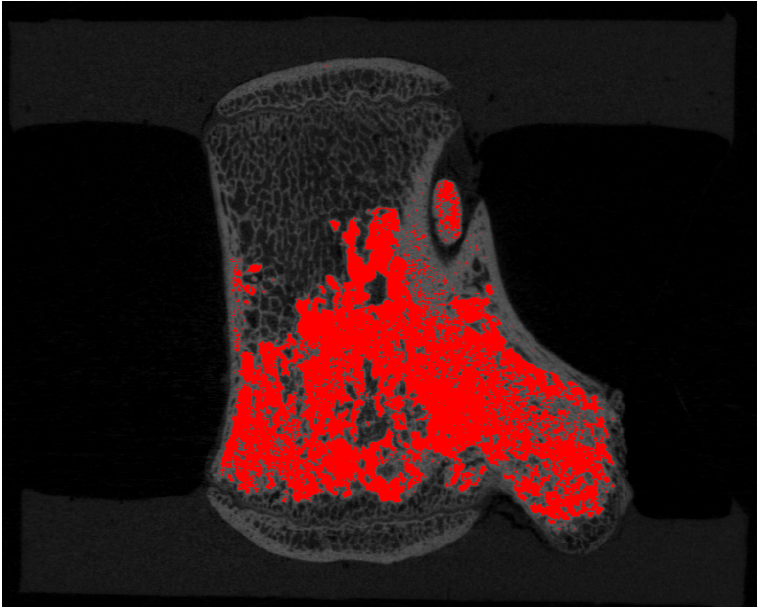
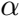


Figure 2.2.4: A lateral slice through an augmented bovine tail vertebra, showing the cement mask in red.

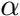
2.2 Material Properties

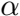


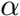


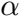


$E_{\text{el}} = \alpha G_S(G_P)$









2.2.1 Properties of Specified Material

2.2.3 Sensitivity Tests

2.2.3.1 Mesh Size Sensitivity

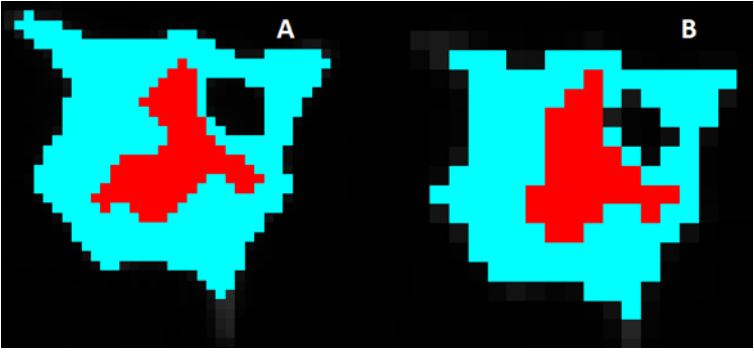


Figure 2.2.5: Mid-slice through an augmented vertebra, cyan: vertebral body, red: cement. A, element size of $1 \times 1 \times 1$ mm. B, element size of $2 \times 2 \times 2$ mm.

2.3.2 Additional cement

Additional information about the data



Table 2.2.1: The difference between interaction properties, tied and not tied for four augmented vertebrae specimens.

Vertebrae (Tail Number, Vertebral Level)	Tied Interaction (N/mm)	No Tied Interaction (N/mm)	Difference (%)
T2 CC1	5496	5496	0
T2 CC2	8086	8086	0.001
T6 CC1	3686	3686	0.001
T4 CC3	6059	6059	0.0005

2.4 Results

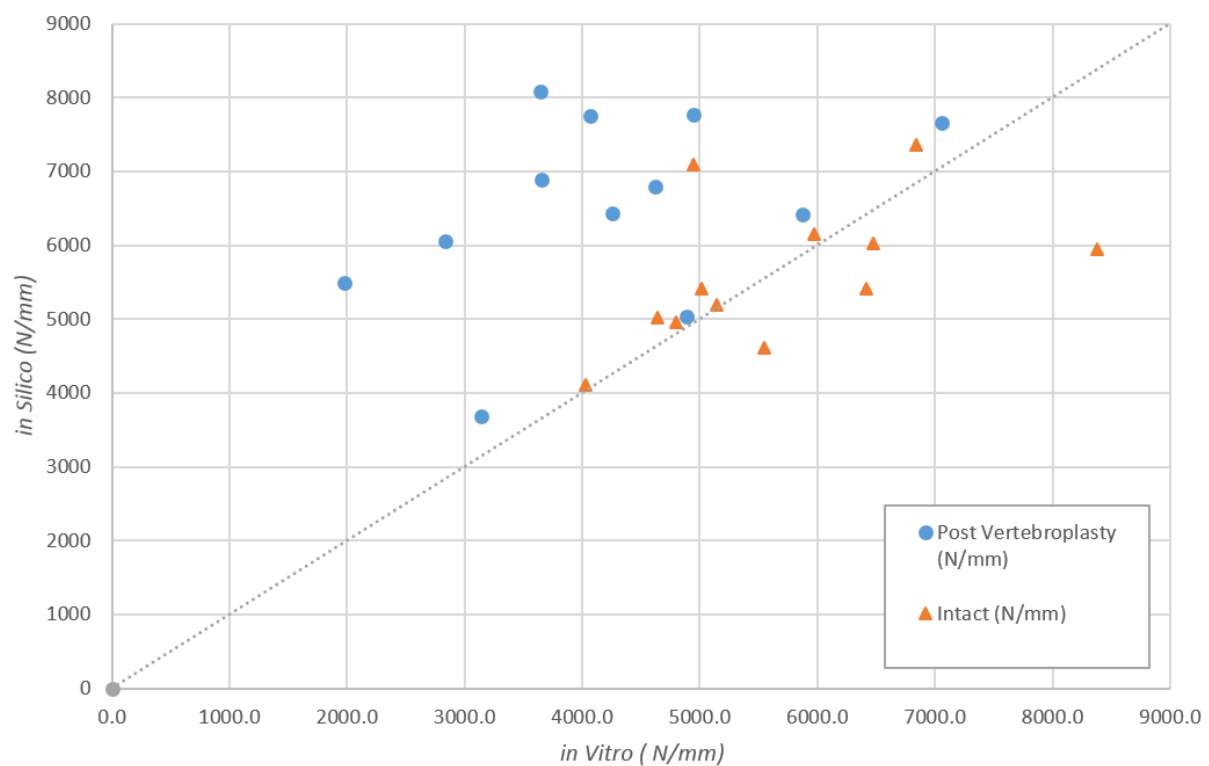
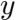
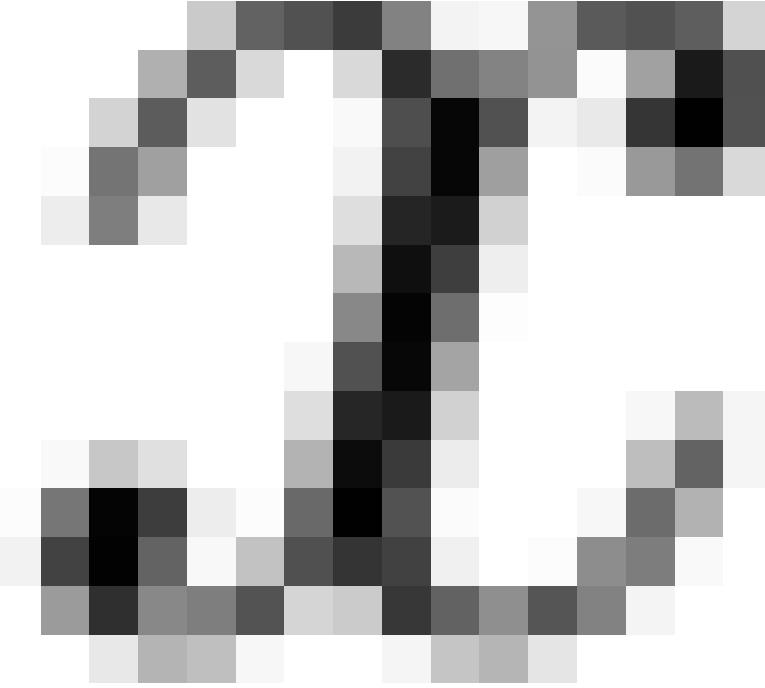


Figure 2.2.6: *in silico* compared with *in vitro* stiffness for intact specimens (triangles) and augmented specimens (circles). The dotted line shows a one-to-one correspondence.

Table 2.2.2: The mean, standard deviation and concordance correlation coefficient (CCC) of the intact and augmented vertebrae for *in vitro* and *in silico* results.

Intact Specimens	Mean Stiffness	Standard Deviation	CCC
<i>in vitro</i>	5684	1196	0.4895
<i>in silico</i>	5610	958	
Augmented Specimens			
<i>in vitro</i>	4246	1371	0.1548
<i>in silico</i>	6507	1298	



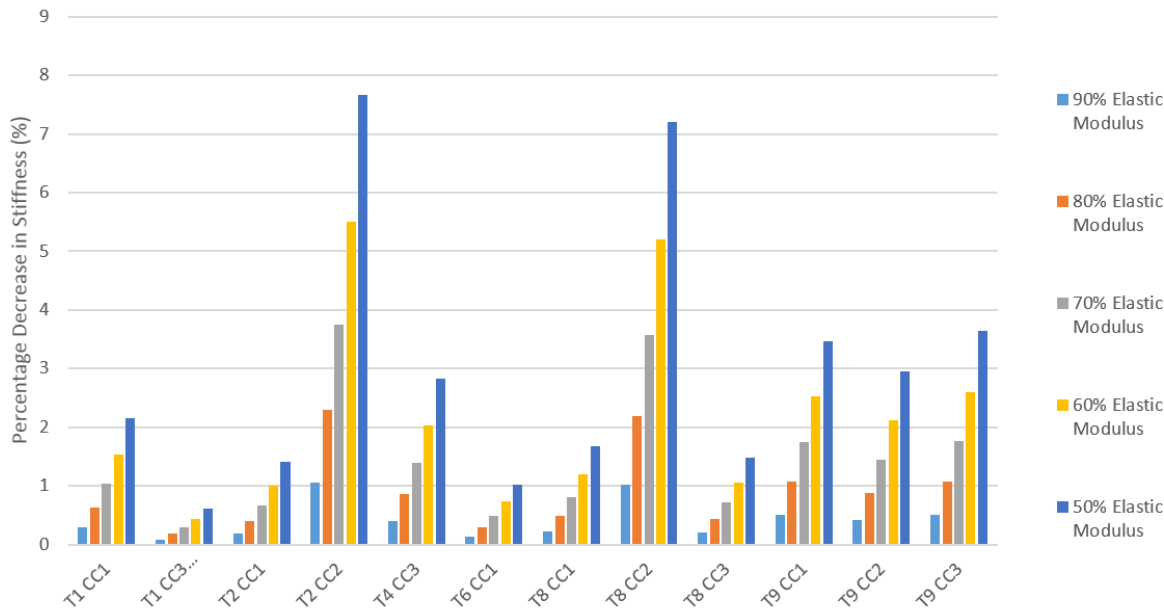


Figure 2.2.7: The percentage decrease in the vertebral stiffness after reducing the elastic modulus of the cement volume within 12 augmented vertebrae.

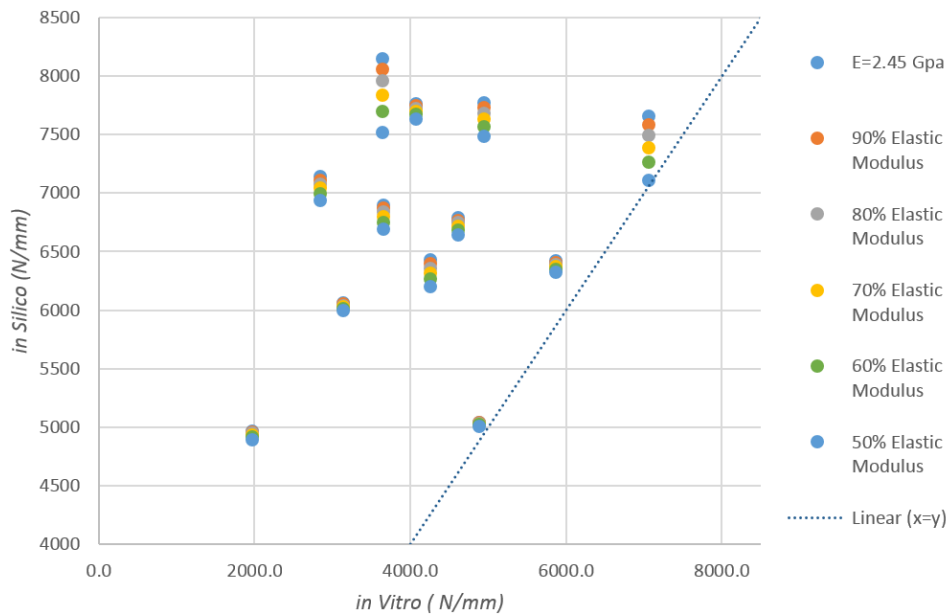


Figure 2.2.8: The effect of reducing the elastic modulus of the cement volume within 12 augmented vertebrae. Shows the *in silico* stiffness for the six elastic moduli tested against their *in vitro* stiffness.

2.2.5 Discussion

Chapter 3

Human Tissue

3.1 Introduction

3.2 Methods

3.2.1 Potting

3.2.2

3.2 Loading

3.2.1 Measures of Classification Stiffness Measurement

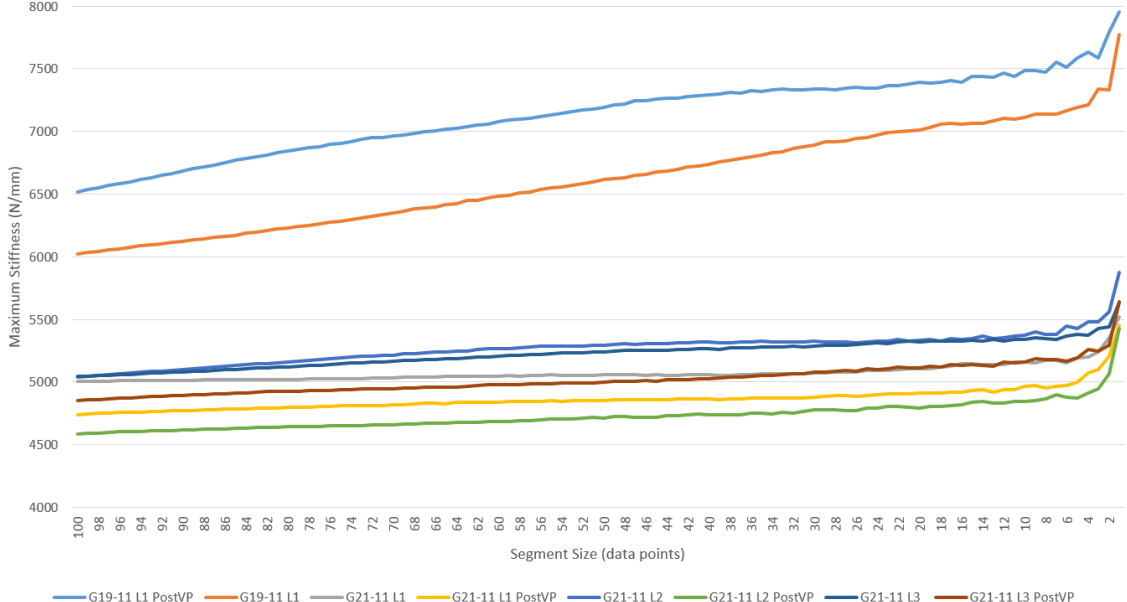


Figure 3.2.1: The effect of reducing the segment size on the maximum stiffness reported from four human vertebrae loaded to 2000 N pre and post augmentation. Using an increment size of 1 data point (0.0017 mm) and segment sizes of 100 to 1 data point (0.17 mm to 0.0017 mm).

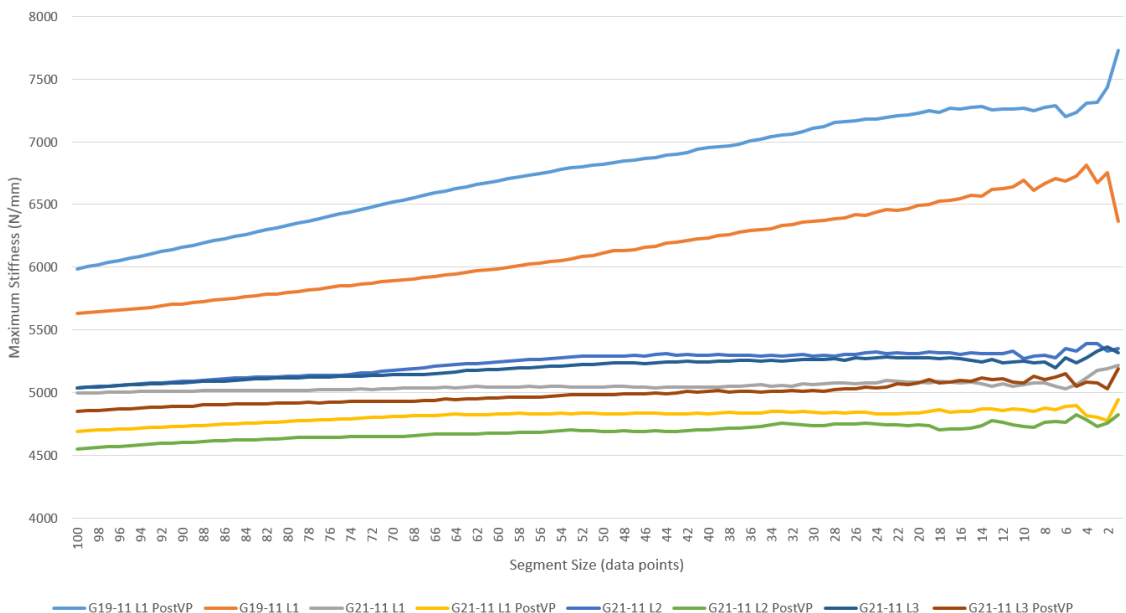


Figure 3.2.2: The effect of reducing the segment size on the maximum stiffness reported from four human vertebrae loaded to 2000 N pre and post augmentation. Using an increment size of 20 data points (0.0037 mm) and segment sizes of 100 to 1 data point (0.17 mm to 0.0017 mm).

3.2.2 Repeated Loading

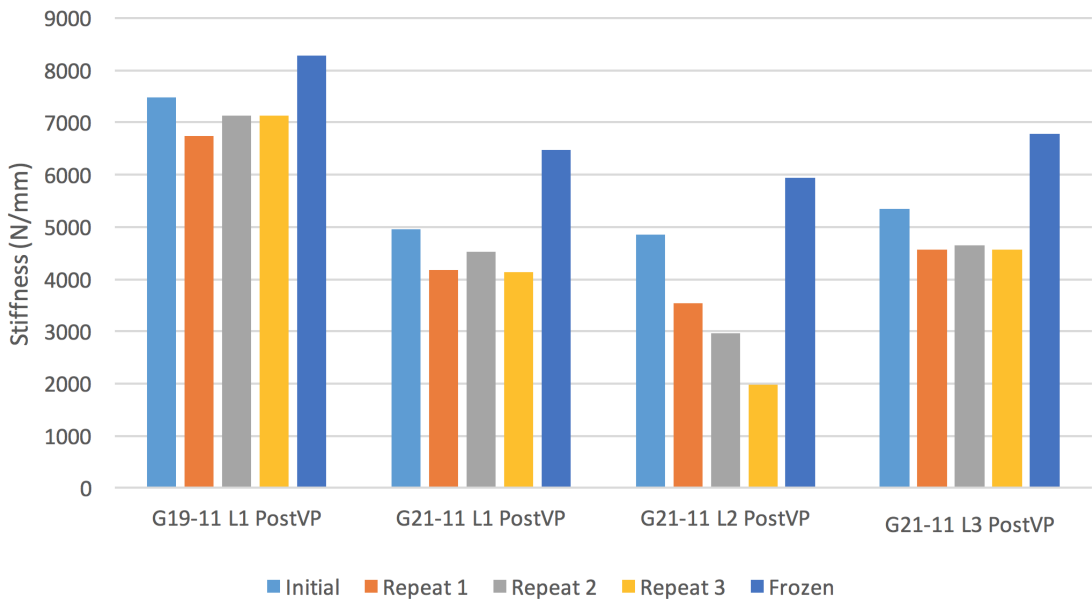


Figure 3.2.3: The stiffness of four augmented vertebral specimens over the course of an initial load, three repeated loads and a load while frozen. The intact specimen was loaded until 2000 N while the remaining four were loaded until 1600 N.

G19-11 L1

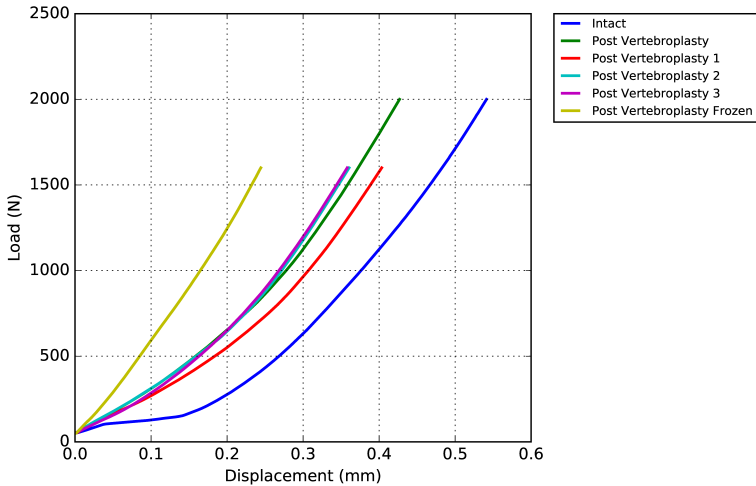


Figure 3.2.4: The load - displacement results for the G19-11 L1 vertebra. Showing results of the intact load and post augmentation load up to 2000 N and the repeats and frozen load up to 1600 N.

G21-11 L1

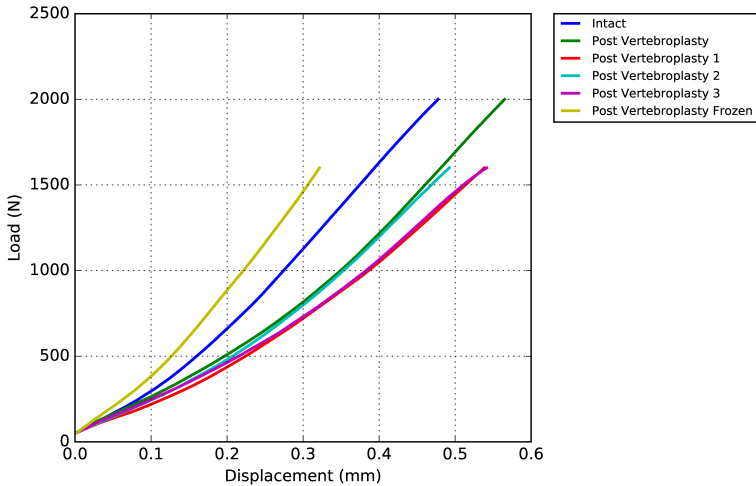


Figure 3.2.5: The load - displacement results for the G21-11 L1 vertebra. Showing results of the intact load and post augmentation load up to 2000 N and the repeats and frozen load up to 1600 N.

G21-11 L2

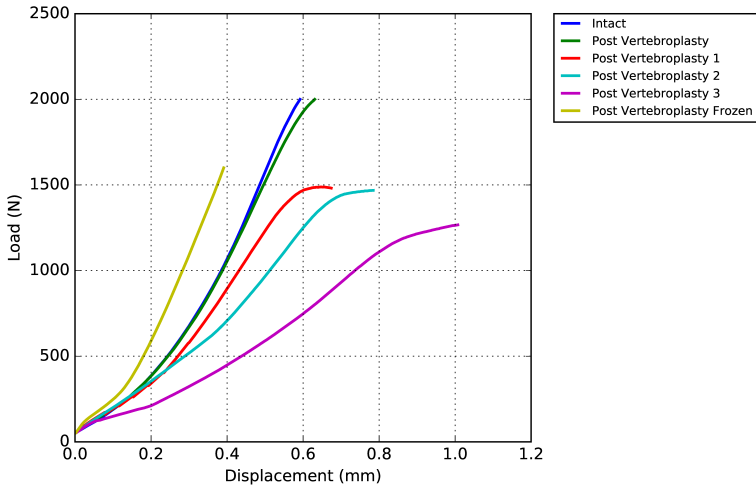


Figure 3.2.6: The load - displacement results for the G21-11 L2 vertebra. Showing results of the intact load and post augmentation load up to 2000 N and the repeats and frozen load up to 1600 N.

G21-11 L3

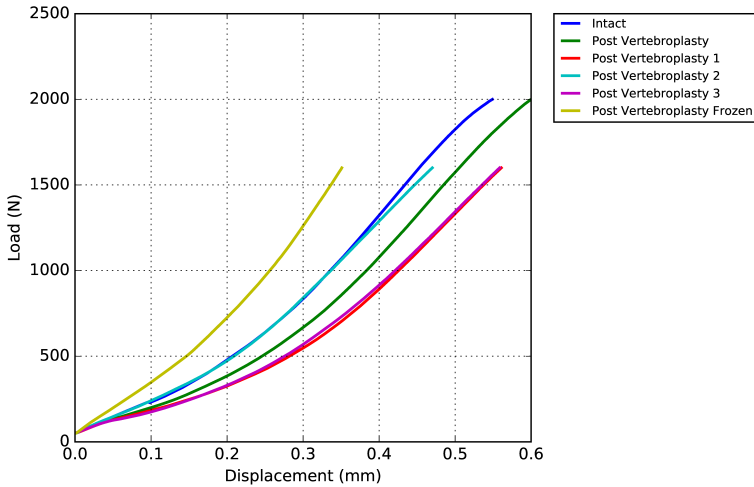


Figure 3.2.7: The load - displacement results for the G21-11 L3 vertebra. Showing results of the intact load and post augmentation load up to 2000 N and the repeats and frozen load up to 1600 N.

3.2.3 Vertebroplasty

3.2.4 Vertebrate characteristics



3.2.4.1 Histograms

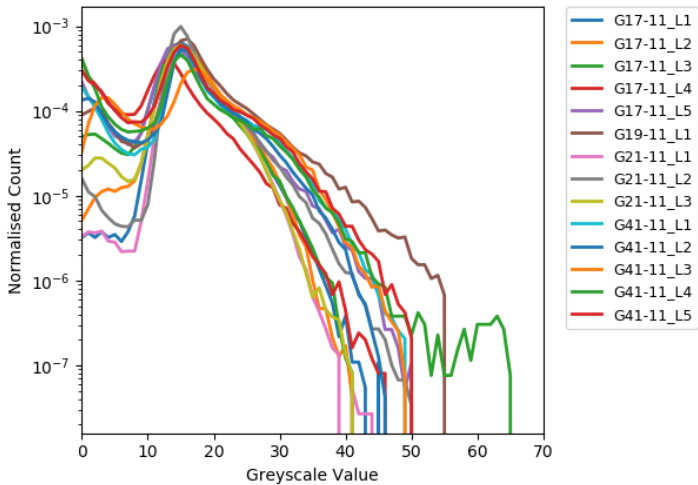


Figure 3.2.8: The normalised (with respect to the volume of the ROI) histogram data for the 14 lumbar vertebrae.



3.2.4.2 Threshold optimisation

3.2.5 Modeling

3.2.5.1 BW/IV Modelling Method

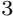
Table 3.2.1: Settings used for the ImageJ plugin, BoneJ: Optimise Threshold.

Options	Values
Tests	11
Range	0.2
Subvolume Size	256
Erosian Cycles	0
Dilation Cycles	0

Table 3.2.2: Threshold and BV/TV values found using the ImageJ plugin BoneJ tools optimise Threshold and Volume Fraction respecively.

Vertebra	Threshold	BV/TV
G19-11 L1	25	0.244
G21-11 L1	22	0.133
G21-11 L2	21	0.107
G21-11 L3	21	0.109





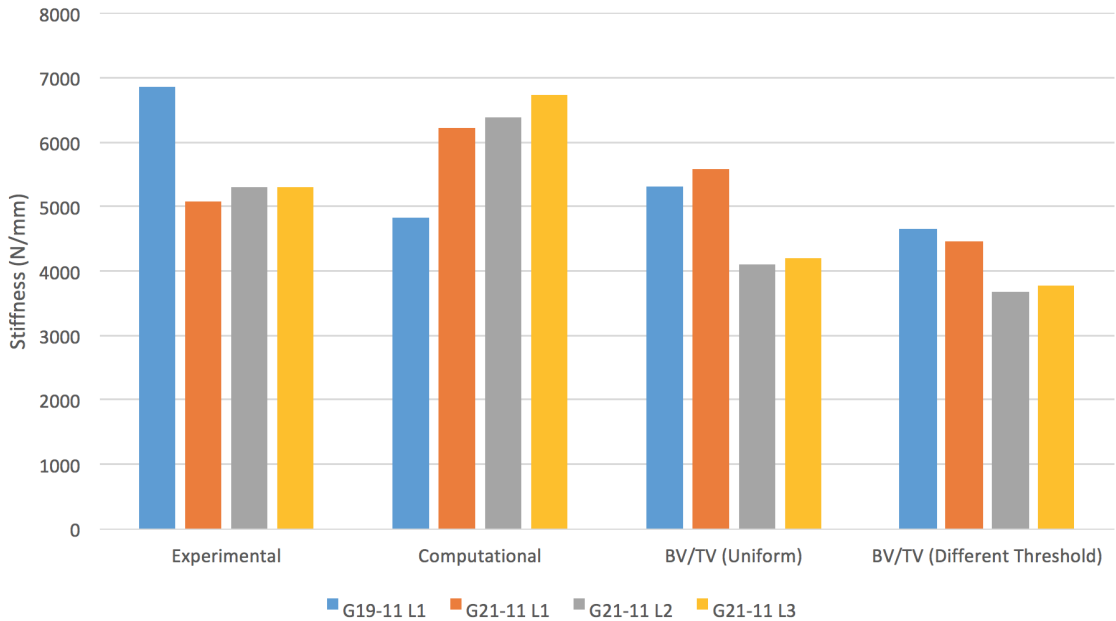


Figure 3.2.9: The stiffness results of three different FE methods for four intact human vertebrae compared to the experimental stiffness results. Interest should be drawn to the ratio between specimen models rather than the values themselves, given that the conversion factors between greyscale values and Young's modulus have not been optimised at this stage. Results show the difference between the currently used method of modelling the vertebrae and the BV/TV based methods (both with uniform thresholds and different thresholds for each specimen).

3.2.6.2 Predicting Vertical Yield Point

3.2.5.3 Load Position Sensitivity

3.3 Results

3.4 Discussion

3.5

Conclusion

Bibliography